A High-Selectivity D-Band Mixed-Mode Filter Based on the Coupled Overmode Cavities

A High-Selectivity D-Band Mixed-Mode Filter Based on the Coupled Over-Mode Cavities

Yi-Wen Wu, *Student Member, IEEE*, Zhang-Cheng Hao, *Senior Member, IEEE*, Rong Lu, *Student Member, IEEE*, and Jia-Sheng Hong, *Fellow, IEEE*

***Abstract*—A D-band low-loss mixed-mode filter with high selectivity is proposed and analyzed in this paper. The transverse quintuplet/triple topology has been employed in the design with coupled over-mode cavities using the $TE_{2N,1,0}$ modes (N=2,3,4…) and $TE_{2N,1,0}$-like modes. Two transmission zeros (TZs) are generated in the upper and lower stopbands. The fractional bandwidth (FBW) and positions of the TZs can be flexibly designed by properly selecting the geometries of the proposed over-mode cavity, which determine the frequencies of all resonating modes. To improve the frequency selectivity, multiple coupled over-mode cavities, which have different spurious responses and TZs distributions, are cascaded for the designed filter. As demonstrations, two types of filter architectures are proposed for two D-band mixed-mode bandpass filters, respectively, which shows the design flexibility of the proposed method. The first filter is realized by cascading multiple over-mode cavities through waveguide sections, and the second filter is realized by cascading over-mode cavities through slots. Experiments are carried out to verify the second filter with TZs. The measured FBW_{3dB} is 17.18% from 128.11 GHz to 152.19 GHz, the minimum insertion loss is around 0.33 dB, and the measured rectangle coefficient (BW_{40dB}/BW_{3dB}) is about 1.38. The measured results agree well with the designed ones, which verifies the proposed method. The proposed filter can be a good candidate for millimeter wave and terahertz systems.**

***Index Terms*—D-band, high selectivity, low insertion loss, mixed-mode filter, over-mode cavity, transverse quintuplet topology, transmission zeros (TZs).**

I. Introduction

RECENTLY, the terahertz (THz) frequency region, loosely ranging from 0.1 to 10 THz, has drawn great attention for the potential applications in the security imaging, biological sensing, ultra-high speed communication, precision radars, and astronomy [1]-[10] due to its wideband spectrum, high spatial and temporal resolution. With the prosperous development of THz science and technology, the THz filter as an essential component in THz systems, has been extensively investigated [11]-[14]. Based on liquid crystals, photonic crystals, metamaterials and frequency-selective surfaces (FSS), a number of THz filters have been studied in [15]-[20]. These filters are exclusively for filtering free-space THz waves in the quasi-optical systems. With the advancement of low-temperature co-fired ceramic (LTCC) technology and micromachining technologies, THz filters based on coupling matrix theory have been reported [21]-[24]. Two 150 GHz LTCC filters with negative and positive couplings, which are realized by different coupling apertures, are illustrated in [21]. The insertion loss of five-pole Chebyshev filter is 8.4 dB with 1.31% FBW and the insertion loss of four-pole quasi-elliptic filter can be reduced to 5.5 dB with 1.35% FBW by removing a resonant cavity and introducing two transmission zeros. In [22], [23], 140 GHz fourth-order and third-order filters with cascaded nonuniform slotted-SIW-based electromagnetic bandgap (EBG) units are demonstrated. The measured minimum insertion losses are 2.44 dB and 1.91 dB, respectively. By adopting the quasi-TE_{111} mode of circular-SIW cavity and the TE_{130}, TE_{140} modes of the over-mode SIW cavity, a fourth-order filter with the minimum insertion loss of 1.9 dB at 174 GHz is investigated in [24]. The LTCC THz filter has a planar form and a low cost. However, its dramatically increased insertion loss is a challenge for the terahertz filter implementation.

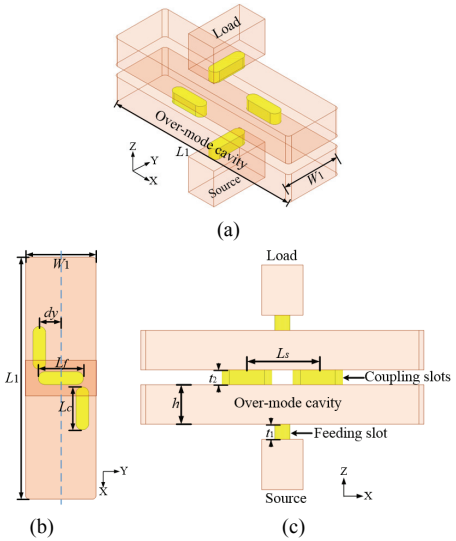

Fig. 1. Basic block of the proposed filter. (a) 3D structure. (b) Top view (xy-plane). (c) Side view (xz-plane).

Nowadays, metallic waveguides are popularly adopted for designing high performance THz filter due to its merits of high quality factor and simple fabrication. Based on different micromachining techniques, such as Si deep reactive ion etching (DRIE) [25]-[27], SU-8 photoresist technology [28]-[31], and computer numerical control (CNC) metal-milling technology [32]-[36], a few THz filters have been reported with a low insertion loss. For example, the insertion loss of a D-band 5-pole filter is 0.61 dB with 10.39% FBW_{3dB} in [25], the measured insertion loss of a 400 GHz silicon micromachined filter with elliptic cavities is up to 2.84 dB with 7.52% FBW_{3dB} in [26], and a 570 GHz silicon micromachined three-pole waveguide filter has a 0.9-dB insertion loss in [27]. The SU-8 photoresist technology shows promising advantages for the implementation of the THz filter [28]-[31]. For example, the measured minimum insertion loss of a 300GHz fifth-order waveguide filter is around 1 dB with 8% FBW_{3dB} in [30].

Apart from the above two technologies, the precision CNC machining technology is also a promising candidate for realizing high performance THz waveguide devices [32]-[36]. Following rapid

Manuscript received Month DD, YYYY; revised Month DD, YYYY; accepted Month DD, YYYY.

This work was supported in part by the National Natural Science Foundation of China 61471118 and 61501114. (*Corresponding Author: Zhang-Cheng Hao*)

Yi-Wen Wu, Zhang-Cheng Hao and Rong Lu are with the state key lab of millimeter-waves, School of Information Science and Engineering, Southeast University, China, and the Purple Mountain Laboratories, Nanjing, China. (e-mail: ywwu@seu.edu.cn, zchao@seu.edu.cn, lurong@seu.edu.cn).

Jia-Sheng Hong is with the School of Engineering and Physical Sciences, Heriot-Watt University, Edinburgh, EH14 4AS, U.K. (e-mail: J.Hong@hw.ac.uk).

development of the precision CNC machining technology, CNC machined waveguide components with high performance have been developed. For example, the insertion loss of the 257.7 GHz filter based on cross coupling is about 0.7 dB with 8.77% FBW_{3dB}, while the 256.3 GHz filter based on modal bypass coupling has a insertion loss of around 0.5 dB with 9.83% FBW_{3dB} [34]. In [35], a 220-GHz fourth-order quasi-elliptic filter fabricated by CNC metal-milling technology exhibits a 0.6-dB insertion loss and 9.8% FBW_{3dB}. By utilizing mode cancellation technology between the spurious mode and dominant mode, a 140 GHz fifth-order filter with two TZs has a 0.52-dB insertion loss and 9.29% FBW_{3dB} [36]. Generally, a good insertion loss is achieved in [33]-[36]. However, their design becomes much complex if a wide stopband suppression and a high selectivity are desired, which also leads to an increased cost. Moreover, different to the DRIE and SU-8 technologies which can afford a fabrication tolerance up to a few micrometers, special considerations still have to be taken for the CNC machining technology due to its cost and fabrication tolerance limitation. For example, a simple filter topology and a relative large coupling slot would be helpful to improve the CNC implementation quality.

In this paper, we proposed a high selective THz mixed-mode filter with simple structure and design process. And higher order filters are realized by cascading multiple over-mode cavities through waveguide sections or slots [37]-[39]. The FBW and the TZs' distributions can be flexibly adjusted by properly selecting the geometries of the over-mode cavity, which determine the distributions of corresponding resonating modes. Section II describes the operating mechanism of the basic over-mode filter block. The determination of the positions of TZs and FBW are presented, and some empirical formulas are given for determining the initial geometries of the basic filter block. In Section III, two 140 GHz bandpass prototypes with high selectivity are designed for demonstrations. Section IV presents experimental results for verifications, as well as comparisons between the proposed filter and relative works in literatures. Finally, Section V draws a conclusion.

II. Mechanism of the Proposed Over-Mode Cavity

A. Basic Configuration and Topology

As indicated in Fig. 1, the basic block for the proposed filter is the coupled over-mode cavities, which consists of two cavities and a few slots. The input/output is the standard WR06 waveguide for 140 GHz applications, and feeding slots are etched at the top/bottom center of two cavities. Those resonant cavities are designed with an even-order mode, i.e. $TE_{2N,1,0}$ (N=2,3,4…), at the center frequency of the bandpass filter by properly turning the dimensions of the cavities (L_1 and W_1). The height of the cavities is 0.78mm, which is similar to the standard WR06 waveguide. Between those two cavities, two slots are used for implementing the inter-coupling. Fig.2 shows the electromagnetic field distributions for different resonate modes of the proposed cavity. Different to the conventional low frequency applications, relatively large electrical sizes have to be adopted for coupling slots to ensure the CNC fabrication quality. Thus, two degenerated even-order modes, shown in Fig. 2b and 2d, appear near the conventional even-order mode shown in Fig. 2c. Since the proposed resonator is composed by two slot-coupled rectangular cavities, those three even-order modes have very similar electromagnetic field distribution, as shown in Fig. 2(b)-(d).

Fig. 3 illustrates the full-wave simulated S-parameters of the basic structure in Fig. 2 for the proposed filter with weak excitations. Five resonance points can be founded in Fig. 3, which indicates five resonate modes are involved in the filter design. To clearly descript

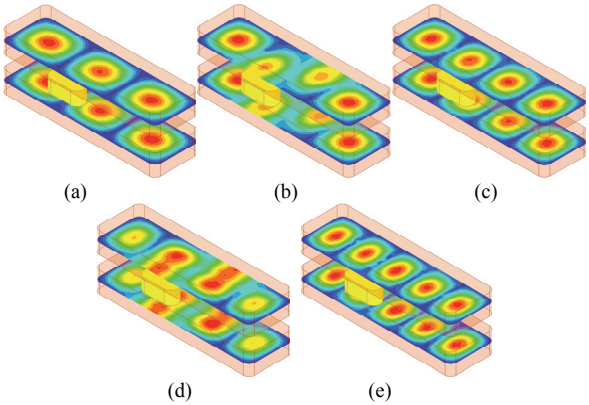

Fig. 2. Electrical field distributions of resonating modes by eigenmode simulation in HFSS. (a) TE_{310} mode at 120.7 GHz. (b) R_1 mode at 130.6 GHz. (c) TE_{410} mode at 140.2 GHz. (d) R_5 mode at 149.2 GHz. (e) TE_{510} mode at 161.2 GHz. ($2N = 4$, $W_1 = 1.64$ mm, $L_1 = 5.64$ mm, $h = 0.78$ mm, $t_2 = 0.5$ mm, $L_s = 1.41$ mm, $L_c = 1.22$ mm, $dy = 0.52$ mm)

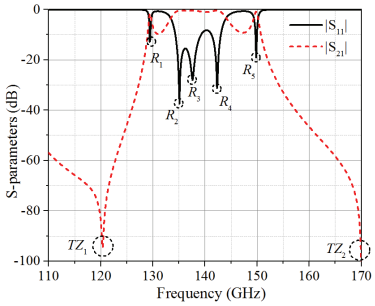

Fig. 3. Simulation response of the proposed structure in Fig. 2 with weak excitations.

those resonate modes, we name those resonate modes as R_1 (at 129.4 GHz), R_2 (at 135.1 GHz), R_3 (at 137.6 GHz), R_4 (at 142.3 GHz), and R_5 (at 149.8 GHz), respectively. In addition, the electric field distributions of those resonant modes are presented in Fig. 4. Obviously, two more resonant modes are obtained under weakly coupled excitation. Moreover, the signs of the vector electric field distributions of the R_1, R_3, R_5 modes at the input (S) and output (L) ports are the same in Fig. 4(a), (c) and (e). Hence, the input and output couplings have the same amplitude and sign ($M_{s1} = M_{1L}$, $M_{s3} = M_{3L}$, and $M_{s5} = M_{5L}$). On the contrary, the input and output couplings of the R_2 and R_4 modes have different signs ($M_{s2} = -M_{2L}$, $M_{s4} = -M_{4L}$) according to the vector electric field distributions in Fig. 4(b) and (d). Consequently, the transversal quintuplet topology in Fig. 5 can be implemented by these five resonators.

B. Study of the Coupling Coefficients

The transversal quintuplet topology based on the quintuplet modes cavity can generate five poles within the passband as well as TZs in the upper and lower stopbands. What can be clearly seen in Fig. 3 is: $f_1 < f_2 < f_3 < f_4 < f_5$. Hence, the resonant frequencies (f_1 and f_5) of the R_1 and R_5 modes determine the bandwidth (BW) of the proposed filter. In addition, a TZ located in the lower stopband is generated when $M_{s2} > M_{s1}$ (and $M_{2L} > M_{1L}$), and a TZ located in the upper stopband is generated when $M_{s4} > M_{s5}$ (and $M_{4L} > M_{5L}$) [38]. Fig. 6 reveals the extracted coupling coefficients M_{s1}, M_{s2}, M_{s3}, M_{s4}, and M_{s5} versus different geometries of feeding slot. Apparently, the coupling coefficients have a steady fall as the height (t_1) of feeding slot increases. In addition, the coupling coefficients M_{s2}, M_{s3}, and M_{s4} are similar, and so are the coupling coefficients M_{s1} and M_{s5}. Furthermore, the input and output couplings satisfy the following relation: $M_{s2} \approx$

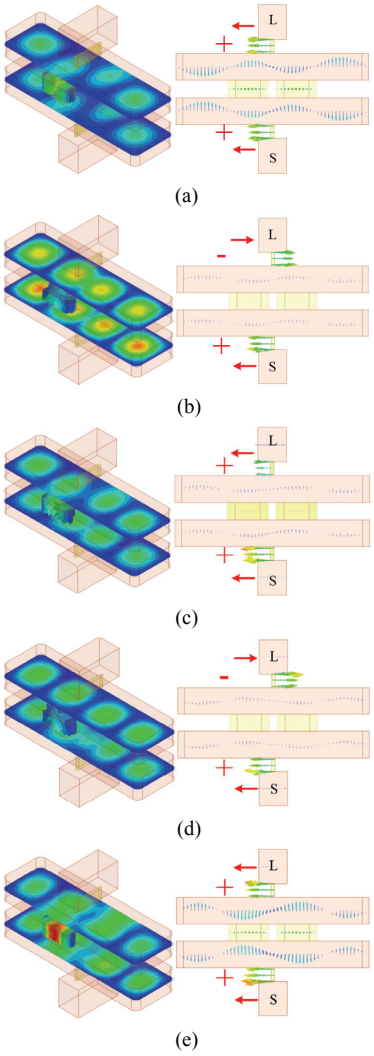

Fig. 4. Electrical field distributions of resonant modes in Fig. 3. (a) R_1 at 129.4 GHz; (b) R_2 at 135.1 GHz; (c) R_3 at 137.6 GHz; (d) R_4 at 142.3 GHz; (e) R_5 at 149.8 GHz. (Red arrow: the direction of vector electric field of the input/output port.)

$M_{s3} \approx M_{s4} > M_{s1} \approx M_{s5}$. Hence, the TZs located in the upper and lower stopbands respectively are generated based on the characters of the transverse quintuplet topology.

As depicted in Fig.4, since the field distribution in each cavity is similar to that of the $TE_{4,1,0}$ mode, the resonant frequencies can be estimated by using a few formulas. Supposing the proposed filter is operated with a center frequency of f_0, the length (L_1) of the over-mode cavity is designed as $N\lambda_{g0}$ at f_0 to keep the dominant $TE_{2N,1,0}$ (N=2,3,4…) mode resonating at center frequency when the width (W_1) of the over-mode cavity is chosen, which can be calculated by (1)-(3). For example, if W_1 is chosen as 1.64 mm, L_1 should be $2\lambda_{g0}$, i.e. 5.64 mm, for obtaining the $TE_{4,1,0}$ resonating mode at 140 GHz.

$$\lambda_0 = \frac{c_0}{f_0}, \qquad \lambda_{g0} = \frac{\lambda_0}{\sqrt{1-(\frac{\lambda_0}{2W_1})^2}} \tag{1}$$

$$L_1 = N\lambda_{g0}, \qquad N= 2,3,4,\ldots \tag{2}$$

$$L_s = \frac{\lambda_{g0}}{2} \tag{3}$$

where c_0 is the speed of light in vacuum, f_0 is the center frequency,

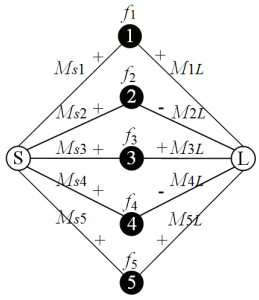

Fig. 5. Transverse quintuplet topology: resonators 1, 2, 3, 4 and 5 represent R_1 mode at f_1, R_2 mode at f_2, R_3 mode at f_3, R_4 mode at f_4, and R_5 mode at f_5, respectively.

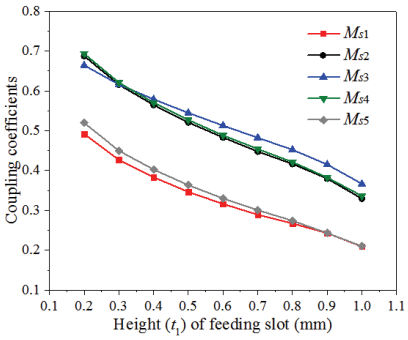

Fig. 6. Extracted input coupling coefficients.

W_1 is the width of the over-mode cavity, L_1 is the length of the over-mode cavity, and L_s is the distance between two coupling slots.

Due to the limitation of the available CNC metal-milling technology, wide coupling slots have to be adopted in the design to relax manufacturing tolerances, which have a width of 0.5 mm, i.e. around one third of the width of the cavity. Consequently, degenerated $TE_{2N,1,0}$-like (N=2,3,4…) modes are generated inside each cavity, of which the resonant frequencies determine the BW of the proposed filter. Due to the large thickness of the feeding slot, it works like a waveguide. Therefore, the cut-off frequency determined by the length (L_f) of the feeding slot should be lower than the passband of the filter. When the cut-off frequency is set at 120 GHz, the L_f is 1.25 mm. To simplify the design, empirical formulas (4)-(7) can be adopted for determining the initial geometries of the cavity for a given filter bandwidth. The width (W_1) and length (L_1) of the cavities are initially determined by two conditions: (a) around the center frequency, those cavities are resonated with the standard even-order modes, i.e. $TE_{2N,1,0}$ (N=2,3,4…); (b) the given bandwidth is equal to the frequency interval of two degenerated modes, i.e. $BW = f_{R_5} - f_{R_1}$. A few empirical formulas have been developed to speed up the initial design. As shown in Fig. 2, according to the eigenmode simulation in the HFSS, the R_1 mode appears between $TE_{3,1,0}$ ($TE_{2N-1,1,0}$) mode and $TE_{4,1,0}$ ($TE_{2N,1,0}$) mode. Hence, the resonant frequency of R_1 mode is estimated by the empirical formula (5). In the similar way, the resonant frequency of R_5 mode is estimated by the empirical formula (6), because R_5 mode appears between $TE_{4,1,0}$ ($TE_{2N,1,0}$) mode and $TE_{5,1,0}$ ($TE_{2N+1,1,0}$) mode. In addition, the spurious passbands appear at the resonating frequencies of other standard even-order modes, such as $TE_{2(N-1),1,0}$ and $TE_{2(N+1),1,0}$, which can be evaluated by (4).

$$f_{TE_{m,1,0}} = \frac{c_0}{2}\sqrt{\left(\frac{m}{L_1}\right)^2 + \left(\frac{1}{W_1}\right)^2}, \qquad m= 1, 2, \ldots \tag{4}$$

$$f_{R_1} = \frac{c_0}{2}\sqrt{\left(\frac{2N-0.5}{L_1}\right)^2 + \left(\frac{1}{W_1}\right)^2}, N = 2, 3, 4, \ldots \quad (5)$$

$$f_{R_5} = \frac{c_0}{2}\sqrt{\left(\frac{2N+0.5}{L_1}\right)^2 + \left(\frac{1}{W_1}\right)^2}, N = 2, 3, 4, \ldots \quad (6)$$

$$\mathrm{FBW} = \frac{f_{R_5} - f_{R_1}}{f_0} \times 100\% \quad (7)$$

where c_0 is the speed of light in vacuum, W_1 and L_1 are the width and length of the cavities. $f_{TE_{m,1,0}}$, f_{R_1} and f_{R_5} are the resonating frequencies of the standard modes, i.e. R_1 and R_5 modes, respectively. And FBW is the fractional bandwidth of the bandpass filter.

Although the bandwidth of the proposed filter is mainly determined by the length (L_1) and width (W_1) of the resonators, the dimensions of coupling slots (dy and Lc) can be used to adjust the self-coupling coefficients of each mode, which affects the filter bandwidth as well. To demonstrate this, the self-coupling coefficients of each mode have been investigated by using full-wave parameter studies, as shown in Fig. 7. As clearly indicated in Fig. 7(a), a larger offset (dy) of the coupling slots leads to larger $|M_{1,1}|$ and $|M_{5,5}|$, which results in a larger resonance frequency separation and wider passband. On the other side, a larger length (Lc) of the coupling slots causes the increase of $M_{1,1}$, $M_{3,3}$, and $M_{5,5}$, as shown in Fig. 7(b). As a result, the passband shifts to a lower frequency. In addition, $M_{2,2}$ and $M_{4,4}$ keep nearly unchanged in Fig. 7(a)-(b). Unfortunately, the coupling of each mode can not be tuned independently to the others, as shown in Fig. 7. A non-independent control of self-coupling limits the degrees of freedom of the design a little bit. However, the selection of the desired band is still possible by designing the mode resonance frequency. Hence, the proposed structure provides a simple and efficient way for the THz filter design. Moreover, the implement of relatively large cavities and slots reduces the fabrication difficulty at THz band and improves the fabrication reliability.

To verify the proposed method, three filters with different FBW_{1dB} are illustrated in Figs. 8-10 and Tables I-III by properly selecting the width (W_1) and the standard even-order resonating mode ($\mathrm{TE}_{2N,1,0}$ mode). Generally, a larger N or narrower width (W_1) leads to a

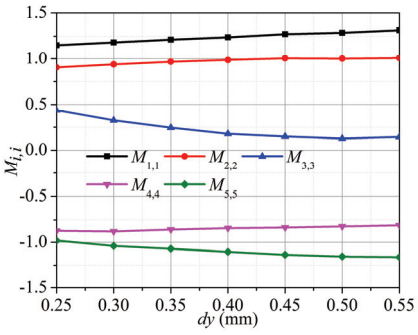

(a)

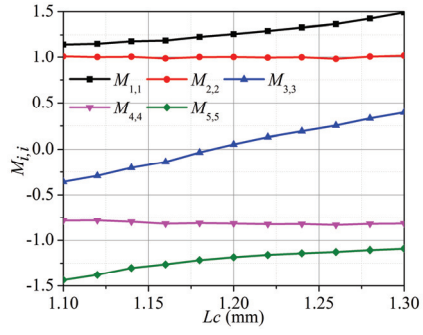

(b)

Fig. 7. Influence of (a) dy and (b) Lc of the coupling slots on the resonant frequencies: M_{11}, M_{22} and M_{33}.

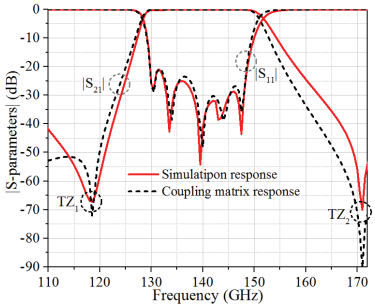

(a)

$$\begin{bmatrix} 0 & 0.358 & 0.525 & 0.551 & 0.548 & 0.381 & 0 \\ 0.358 & 1.288 & 0 & 0 & 0 & 0 & 0.358 \\ 0.525 & 0 & 0.981 & 0 & 0 & 0 & -0.525 \\ 0.551 & 0 & 0 & 0.087 & 0 & 0 & 0.551 \\ 0.548 & 0 & 0 & 0 & -0.844 & 0 & -0.548 \\ 0.381 & 0 & 0 & 0 & 0 & -1.189 & 0.381 \\ 0 & 0.358 & -0.525 & 0.551 & -0.548 & 0.381 & 0 \end{bmatrix}$$

(b)

Fig. 8. First filter block. (a) Comparison between simulation response and coupling matrix. (b) Coupling matrix. (2N = 4, W_1 = 1.64 mm, L_1 = 5.64 mm, h = 0.78 mm, t_1 = 0.4 mm, L_f = 1.25 mm, L_c = 1.22 mm, Ls = 1.41 mm, dy = 0.52 mm, t_2 = 0.5 mm)

TABLE I
COMPARISONS BETWEEN THE DESIGNED AND CALCULATED RESULTS

	TZ_1/GHz	TZ_2/GHz	FBW_{1dB}	P_1/GHz	P_2/GHz
Designed	118.5	170.5	15.2%	103.1	187.2
Calculated	115.6	168.3	14.3%	105.7	183.4

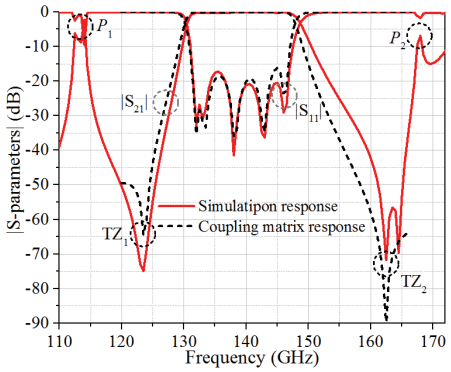

(a)

$$\begin{bmatrix} 0 & 0.334 & 0.495 & 0.527 & 0.505 & 0.334 & 0 \\ 0.334 & 1.301 & 0 & 0 & 0 & 0 & 0.334 \\ 0.495 & 0 & 1.009 & 0 & 0 & 0 & -0.495 \\ 0.527 & 0 & 0 & 0.135 & 0 & 0 & 0.527 \\ 0.505 & 0 & 0 & 0 & -0.764 & 0 & -0.505 \\ 0.334 & 0 & 0 & 0 & 0 & -1.158 & 0.334 \\ 0 & 0.334 & -0.495 & 0.527 & -0.505 & 0.334 & 0 \end{bmatrix}$$

(b)

Fig. 9. Second filter block. (a) Comparison between simulation response and coupling matrix. (b) Coupling matrix. (2N = 4, W_1 = 1.41 mm, L_1 = 6.6 mm, h = 0.78 mm, t_1 = 0.7 mm, L_f = 1.25 mm, L_c = 1.21 mm, Ls = 1.65 mm, dy = 0.27 mm, t_2 = 0.8 mm)

TABLE II
COMPARISONS BETWEEN THE DESIGNED AND CALCULATED RESULTS

	TZ_1/GHz	TZ_2/GHz	FBW_{1dB}	P_1/GHz	P_2/GHz
Designed	123.5	162.5	11.95%	114.4	168
Calculated	122.5	161.4	10.54%	115.7	173

narrower bandwidth. It can be seen that the evaluated bandwidth and spurious passbands from (4)-(7) well predicts those of the designed filter.

C. Field Analysis of the Transmission Zeros (TZs)

As mentioned in part B, the proposed filter with the transversal quintuplet topology can generate two TZs in the upper and lower stopbands respectively, and the locations of TZs can be adjusted appropriately by changing the coupling coefficients of the transversal quintuplet topology. In this design, five resonant modes are excited by the same feeding slot, the adjustable range of ratio M_{s2}/M_{s1} is limited, as revealed in Fig. 6. Hence, the positions of TZs varies within a certain range when the geometries (W_1 and L_1) of the over-mode cavity are determined. On this occasion, the approximate positions of TZs can be estimated according to the geometries of the over-mode cavity.

The electric field distributions of the TZs are depicted in Fig. 11. As presented in Fig. 11(a), the lower cavity is excited by the feeding slot. However, the upper cavity can not be excited through coupling slots. It can be clearly seen from the vector electric field distribution in Fig. 11(b) that the coupling slot is placed on the right top of the out-of-phase part of the two neighboring standing waves. Therefore, the coupling electromagnetic fields are cancelled, which leads to a TZ at lower stopband. This kind of field distribution is caused by the mode cancelling between R_1 mode at f_1 and R_2 mode at f_2 in the transversal quintuplet topology. In the same way, the field distribution of the TZ at upper stopband results from the mode cancelling between R_4 mode at f_4 and R_5 mode at f_5 in the transversal quintuplet topology.

To initially determine the positions of TZs, empirical formulas have been concluded as (8)-(10) according to the field distribution of TZs.

$$L_0 = \frac{L_1 - L_s}{2} = \frac{(2N-1)\lambda_{g0}}{4}, \quad N = 2,3,4,\ldots \tag{8}$$

$$f_{TZ\_lower} = \frac{c_0}{2}\sqrt{\left(\frac{N-1}{L_0}\right)^2 + \left(\frac{1}{W_1}\right)^2}, \; N = 2, 3, 4, \ldots \tag{9}$$

$$f_{TZ\_upper} = \frac{c_0}{2}\sqrt{\left(\frac{N}{L_0}\right)^2 + \left(\frac{1}{W_1}\right)^2}, \quad N = 2, 3, 4, \ldots \tag{10}$$

where L_0 is the distance from the center of coupling slot-1 to the edge of the over-mode cavity, and W_1 is the width of the cavities. f_{TZ_lower} and f_{TZ_upper} are the frequencies of the TZs.

Based on the initial geometries, designed filters have the similar TZ distributions in the Tables I-III, which shows that those empirical formulas are good enough for obtaining the initial geometries of the proposed filter.

III. Design Examples

As shown in Figs. 8-10 and Table I-III, although the basic block of the proposed filter can provide a good passband and selectivity, there are spurious passbands appeared near the lower or upper passband. That decreases the filter performance. To solve this problem, two basic blocks which have different spurious passbands can be integrated to design the proposed bandpass filter for achieving a wide stopband with high rejection level. For a given specification, the design procedure of the proposed filter can be summarized as following:

According to the selected CNC machining process, the miniature width of the feeding slots and coupling slots are chosen to ensure that a good fabrication quality can be achieved. In this design, it is 0.5mm.

(i) According to the given specifications, one can built the first filter block whose geometries, including cavity size, locations of the coupling slots, can be initially obtained from (1)-(10) by properly choosing the fundamental resonating modes and the locations of TZs.

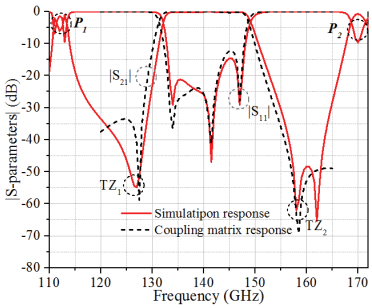

(a)

$$\begin{bmatrix} 0 & 0.431 & -0.605 & 0.619 & -0.586 & 0.377 & 0 \\ 0.431 & 1.497 & 0 & 0 & 0 & 0 & 0.431 \\ 0.605 & 0 & 1.303 & 0 & 0 & 0 & -0.605 \\ 0.619 & 0 & 0 & 0.268 & 0 & 0 & 0.619 \\ 0.586 & 0 & 0 & 0 & -0.801 & 0 & -0.586 \\ 0.377 & 0 & 0 & 0 & 0 & -1.241 & 0.377 \\ 0 & 0.431 & -0.605 & 0.619 & -0.586 & 0.377 & 0 \end{bmatrix}$$

(b)

Fig. 10. Third filter Block. (a) Comparison between simulation response and coupling matrix. (b) Coupling matrix. (2N = 6, W_1 = 1.64 mm, L_1 = 8.46 mm, h = 0.78 mm, t_1 = 0.5 mm, L_f = 1.25 mm, L_c = 1.21 mm, Ls = 1.41 mm, dy = 0.48 mm, t_2 = 0.5 mm)

TABLE III
Comparisons between the Designed and Calculated Results

	TZ_1/GHz	TZ_2/GHz	FBW_{1dB}	P_1/GHz	P_2/GHz
Designed	127	158	11%	114	170
Calculated	124.7	156.7	9.55%	115.6	168.3

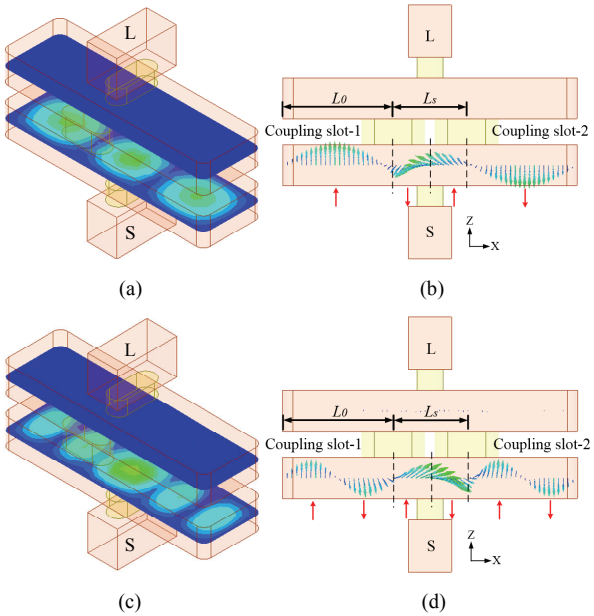

Fig. 11. Field distributions of the TZs. (a) 3D-view and (b) side view (xz-plane) of TZ_1 @ 118.5 GHz. (c) 3D-view and (b) side view (xz-plane) of TZ_2 @ 171 GHz. (Red arrow: the direction of vector electric field in the lower over-mode cavity.)

As introduced in part B of Section II, the geometries are tuned according to the coupling matrix for achieving a good in-band response.

(ii) Following (i), one can built the second filter block whose initial geometries are obtained from (1)-(10). In this step, to extend the stopband, the spurious response and TZs' locations are different to those of the first filter block, and the coupling control and practical tuning based on the coupling matrix are repeated as well. If higher

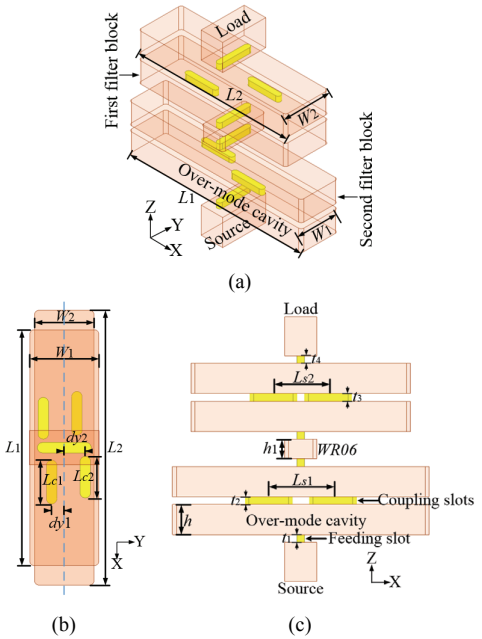

Fig. 12. Configuration of the proposed filter-I. (a) 3D structure. (b) Top view (xy-plane). (c) Side view (xz-plane).

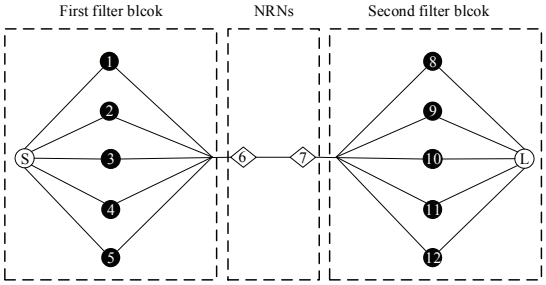

Fig. 13. Coupling topology of the filter-I.

selectivity and wider stopband are desired, this step can be repeated for more filter blocks.

(iii) Cascaded filter blocks built above for the proposed filter. And the full-wave simulator is used to adjust or optimize the filter structure to achieve a good in-band return loss, high selectivity and wide stopband for given specifications.

To show the design process in detail, two filter examples operated with a center frequency of 140 GHz are illustrated in the following with different cascaded topologies.

A. Filter-I

The first filter adopts a series topology using two basic filter blocks, as shown in Fig. 12(a), and its side view and top view are presented in Fig. 12(b) and (c), respectively. The specifications of this filter are:

1. Center frequency: f_0 =140 GHz;
2. FBW_{1dB} =11.5%;
3. In-band reflection coefficient: better than -20 dB;
4. $|S_{21}| \leqslant$ -40 dB within 110-120 GHz and 160-170 GHz.

According to the design procedure mentioned above, the $TE_{4,1,0}$ mode is chosen as the fundamental resonating mode at 140 GHz, which ensures that the cavity has a relatively large size for the CNC machining technology. Due to the same reason, the width of the coupling and feeding slots are chosen as 0.5 mm and the length of slots are 1.25 mm when the cut-off frequency is chosen as 120 GHz. Then,

TABLE IV
GEOMETRIES OF THE PROPOSED FILTER-I (UNIT: MM)

W_1	L_1	L_{f1}	L_{c1}
1.64	5.64	1.25	1.22
h	dy_1	t_1	t_2
0.78	0.5	0.5	0.4
W_2	L_2	L_{f2}	L_{c2}
1.41	6.6	1.25	1.21
h_1	dy_2	t_3	t_4
1	0.27	0.7	0.8

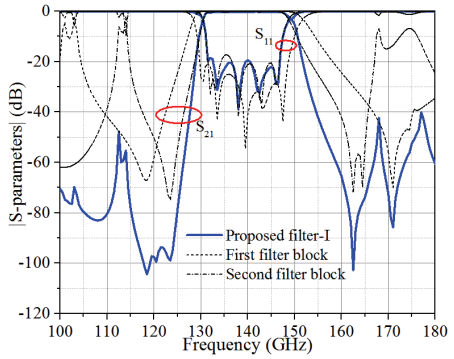

Fig. 14. S-parameters of the proposed filter-I.

the width and length of the over-mode cavity of the first filter block are determined by using (1)-(10) as 1.64 mm and 5.64 mm respectively, which indicates that the TZs are located at 115.6 GHz and 168.3 GHz, and the spurious passbands appear at 105.7 GHz and 183.4 GHz, respectively. The length and offset of the coupling slots are optimized with the HFSS software as L_{c1} = 1.22 mm and dy_1 = 0.50 mm for a good in-band response of the first filter block, as shown in Fig. 8.

To suppress the spurious passbands of the first filter block, the width and length of the second filter block are chosen as 1.41 mm and 6.6 mm by using (1)-(10), which means that the spurious passbands of the second filter block appear at 115.7 GHz and 173 GHz, and the locations of the TZs are 122.5 GHz and 161.4 GHz. The length and offset of the coupling slots are then optimized as L_{c2} = 1.21 mm and dy_2 = 0.27 mm for a good in-band response of the second filter block, as shown in Fig. 9.

As illustrated in Fig. 13, the two designed filter blocks are cascaded together by a WR06 waveguide. By properly adjusting the geometries of slots and WR06 waveguide section in Fig. 12, the filter-I is designed with a high selectivity, and its final geometries are listed in Table IV. The full-wave simulated results for the filter-I are depicted in Fig. 14. It can be seen that the spurious passband of the first and second filter block are well suppressed, and the frequency selectivity is significantly improved. The simulated FBW_{1dB} is about 11.7%, the in-band reflection coefficient is better than -20 dB, the insert loss is around 0.25 dB at 140 GHz, and the rectangle coefficient (BW_{40dB}/BW_{3dB}) is around 1.44, where BW_{40dB} and BW_{3dB} are the 40-dB and 3-dB bandwidths, respectively. From 100-120 GHz and 160-180 GHz, the rejection level is higher than 40 dB.

B. Filter-II

The second filter is realized by cascading two basic single over-mode cavities through TE_{440} mode cavities, as shown in Fig. 15. The specifications of this filter are:

1. Center frequency: f_0 =140 GHz;
2. FBW_{1dB} = 16%;
3. In-band reflection coefficient: better than -10 dB;
4. $|S_{21}| \leqslant$ -40 dB within 110-120 GHz and 160-170 GHz.

The basic block in Fig. 1 is composed of two over-mode cavities and coupling slots, which has five resonant modes and can be represented by the transverse quintuplet topology. However, the basic filter block in Fig. 16(a) consists of only one over-mode cavity, a high-order mode (TE_{440} mode) cavity, and coupling slots. The implement of these higher-mode cavities helps to reduce the insertion loss of the proposed filter, especially for THz applications. It should be mentioned that since the coupling slots on the top of the over-mode cavity have the same offsets, the electromagnetic-fields of the neighboring coupling slots have an out-of-phase. Hence, the single over-mode cavity can provide same-amplitude but alternative-phase excitation for the TE_{40} mode cavity, which ensures only the TE_{40} mode can be resonated inside the high-order mode cavity. To investigate the number of resonate mode of the over-mode cavity, a TE_{40} mode transmission line is connected with the single over-mode cavity as output port, as shown in Fig. 16(a). Then the full-wave simulated reflection coefficient is studied and presented in Fig. 16(b). Apparently, three resonate modes can be observed in Fig.16 (b). The vector electric field distributions of those three modes are depicted in Fig. 17. The signs of vector electric field of the $R_{1'}$ and $R_{3'}$ modes at the coupling slots are the same, but opposite to that of the $R_{2'}$ mode. Hence, it can be represented by a transverse triplet topology, which can generate two TZs.

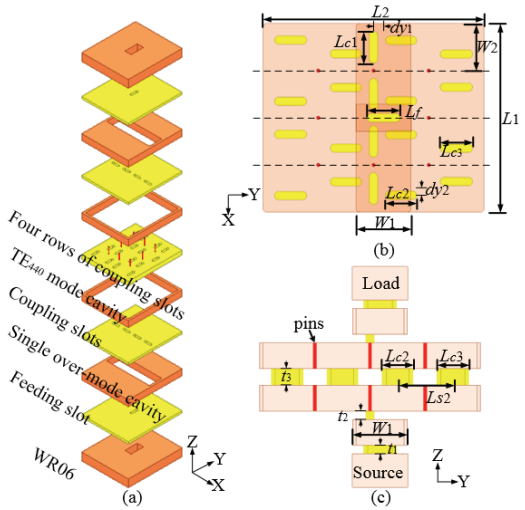

Fig. 15. Configuration of the proposed filter-II. (a) 3D structure. (b) Top view (xy-plane). (c) Side view (yz-plane).

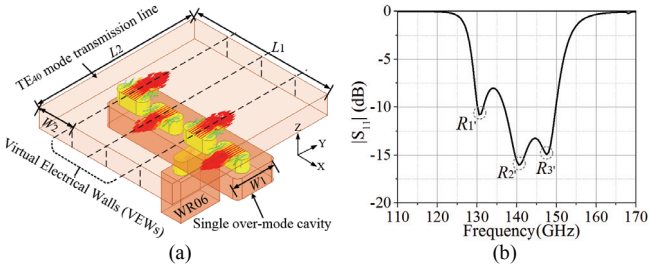

Fig. 16. (a) Basic filter block based on a single over-mode cavity. (b) Reflection coefficient of the TE_{40} mode transmission line excited by the single over-mode cavity.

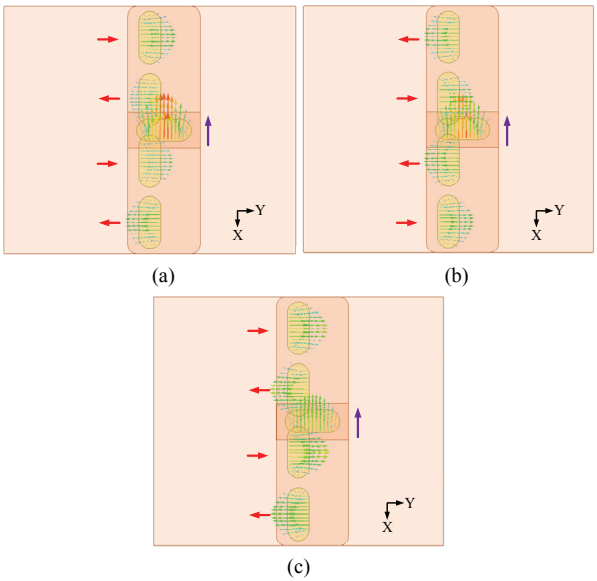

Fig. 17. Vector electric field distributions of the resonant modes in the single over-mode cavity. (a) $R_{1'}$ mode; (b) $R_{2'}$ mode; (c) $R_{3'}$ mode. (Red arrow: the direction of vector electric field of the coupling slot; Purple arrow: the direction of vector electric field of the feeding slot.)

As demonstrated in Fig. 15, two basic filter blocks are cascaded together with 16 slots to improve the frequency selectivity. The topology based on the transverse triplet is displayed in Fig. 18. In order to suppress the unwanted high-order resonating modes within the passband and keep the same resonating characteristics as the conventional over-mode cavity, eight tiny metal pins are placed along

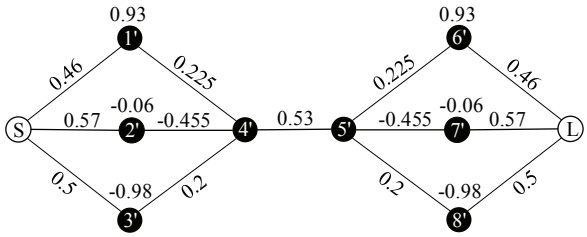

Fig. 18. Coupling topology of the filter-II: resonators 1', 2', and 3' represent the resonant modes in the lower single over-mode cavity, respectively; resonator 4' and 5' represent the TE_{440} modes in the lower and upper TE_{440} mode cavities, respectively; resonators 6', 7', and 8' represent the resonant modes in the upper single over-mode cavity, respectively.

TABLE V
GEOMETRIES OF THE PROPOSED FILTER-II (UNIT: MM)

W_1	L_1	L_f	L_{c1}
1.64	5.64	1.24	1.2
dy_1	Ls_1	t_1	h
0.3	1.41	0.5	0.78
W_2	L_2	L_{c2}	L_{c3}
1.41	6.6	1.18	1.21
dy_2	Ls_2	t_2	t_3
0.2	1.65	0.5	0.9

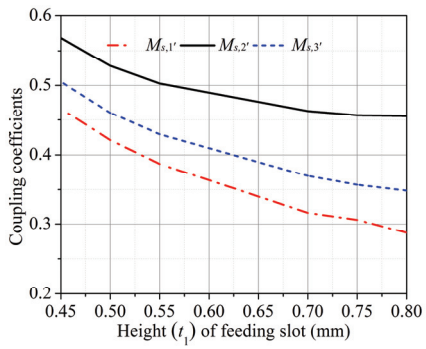

Fig. 19. Extracted input coupling coefficients: $M_{s1'}$, $M_{s2'}$ and $M_{s3'}$.

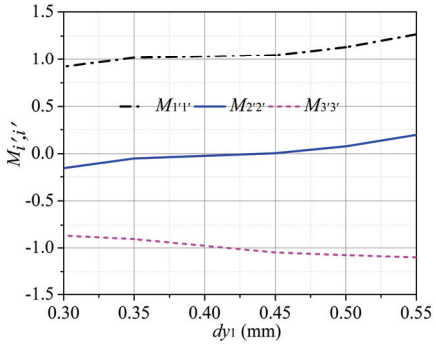

(a)

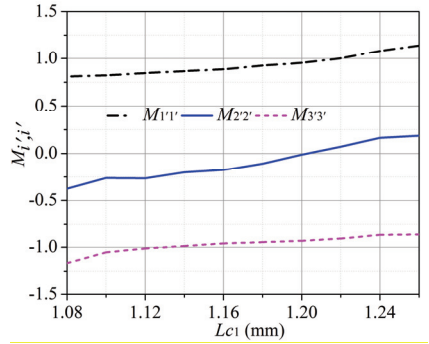

(b)

Fig. 20. Influence of (a) dy_1 and (b) Lc_1 of the coupling slots on the resonant frequencies ($M_{1'1'}$, $M_{2'2'}$ and $M_{3'3'}$).

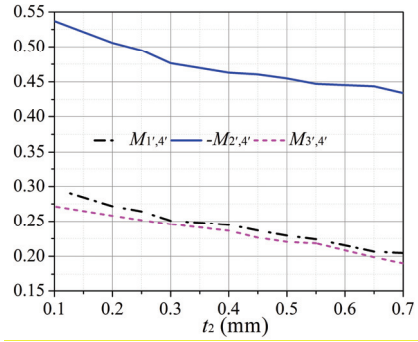

Fig. 21. Influence of t_2 of the coupling slots on the coupling coefficients: $M_{1'4'}$, $-M_{2'4'}$ and $M_{3'4'}$.

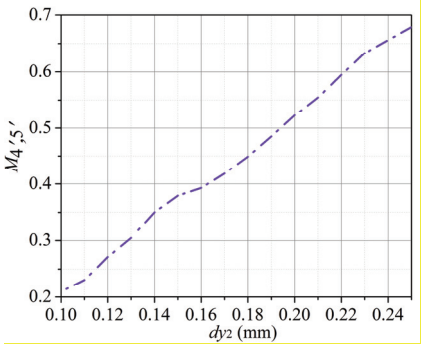

Fig. 22. Influence of dy_2 on $M_{4'5'}$.

the black dash lines in Fig. 15(b). Similar design procedure is adopted to design the proposed filter-II. The geometries of over-mode cavities and TE_{440} mode cavities can be determined by using (1)-(10). The

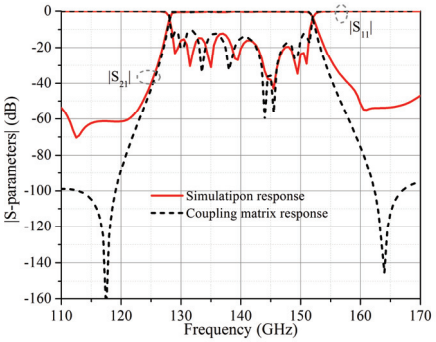

Fig. 23. Comparison between the full-wave simulation responses and the coupling matrix response.

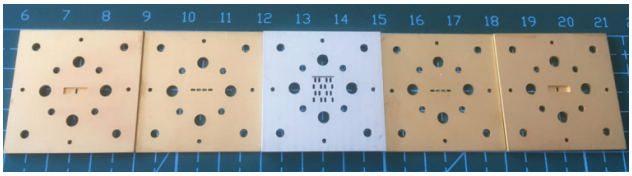

(a)

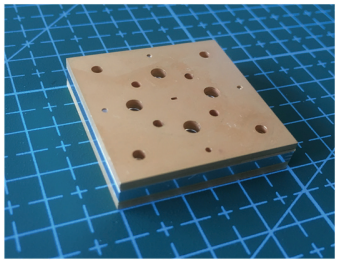

(b)

Fig. 24. Photographs of the filter-II. (a) Unassembled prototype. (b) Assembled prototype.

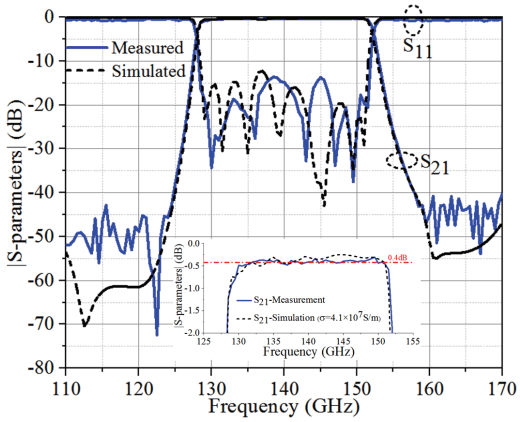

Fig. 25. The measured and simulated results of the proposed filter-II.

coupling matrix in Fig. 18 is used to guide the geometric tuning in the design. As depicted in Fig. 19, the input coupling coefficients monotonically decrease as the height (t_1) of feeding slot increases. For the given center frequency and the bandwidth of a passband filter, the width (W_1) and length (L_1) of the single over-mode cavity should satisfy the formulas (1)-(3) to keep the $TE_{4,1,0}$ ($R_{2'}$) mode resonating at center frequency. Then the resonating frequencies of the $R_{1'}$ and $R_{3'}$ modes can be calculated by formulas (5) and (6) respectively. The self-coupling coefficients of $M_{1'1'}$, $M_{2'2'}$ and $M_{3'3'}$ are investigated with

TABLE VI
COMPARISONS OF PERFORMANCES AMONG THE REPORTED THZ FILTERS

Reference	f_0 (GHz)	FBW_{3dB}	$IL(dB)$	$\frac{BW_{40dB}}{BW_{3dB}}$	Technology	Comments
[21]	149.7	1.35%	~5.5	N.A.	LTCC	4-pole quasi-elliptic
[22]	140	14.28%	~2.44	~2.33	LTCC	Synthesis method based on electric coupling
[23]	140.45	13.03%	~1.91	~2.86	LTCC	Electromagnetic bandgap (EBG) Unit
[24]	174	13.8	~1.9	N.A.	LTCC	SICW resonant cavity
[25]	141.9	10.22%	~0.61	~3.24	DRIE	5-pole Chebyschev
[28]	88.47	9.73%	~0.97	N.A.	SU-8	H-plane bends
[29]	102	5%	~1.2	N.A.	SU-8	Extracted pole resonator
[30]	300	8%	~1	N.A.	SU-8	5-pole Chebyshev
[31]	298.6	5.36%	~0.45	N.A.	SU-8	Extracted pole resonator
	286.6	5.58%	~0.41	~3.21	CNC	Extracted pole resonator
[33]	100	10%	~0.6	~1.9	CNC	Extracted pole resonator
[34]	258	8.8%	~0.7	~1.86	CNC	Higher order mode cavity
	256	9.8%	~0.5	~1.62	CNC	Higher order mode cavity
[36]	140	9.29%	~0.52	~1.47	CNC	TE_{301} mode resonant cavity
Filter-I (Simulated)	**140**	**13.35%**	**~0.25**	**~1.44**	**N.A.**	**Over-mode cavities**
Filter-II	**140**	**17.18%**	**~0.33**	**~1.38**	**CNC**	**Over-mode cavities**

the full-wave parameter study. As presented in Fig. 20(a), a larger offset (dy_1) of the coupling slots causes larger $|M_{1'1'}|$ and $|M_{3'3'}|$, which leads to a larger resonance frequency separation and wider passband. In Fig. 20(b), a larger length (L_{c1}) of the coupling slots results in the increase of $M_{1'1'}$, $M_{2'2'}$, and $M_{3'3'}$, which causes the passband to shift to the lower frequency. In addition, as demonstrated in Fig. 21, the coupling coefficients ($M_{1'4'}$, $-M_{2'4'}$ and $M_{3'4'}$) descends slowly as the height (t_2) of the coupling slots increases. Moreover, $M_{4'5'}$ increases rapidly as the offset (dy_2) increases, as illustrated in Fig. 22.

The final geometries are listed in the Table V, and the simulated S-parameters are presented in the Fig. 23. The simulated FBW_{1dB} is from 128.63 GHz to 151.53 GHz (about 16.35%), the in-band reflection coefficient is better than -12.5 dB, and the TZs are located at 112.5 GHz, 120 GHz, and 161 GHz, respectively. The simulated insertion loss is 0.15 dB at 140 GHz, and the rectangle coefficient (BW_{40dB}/BW_{3dB}) is around 1.39.

IV. FABRICATION AND MEASUREMENT

To verify the design, only the proposed filter-II is fabricated by CNC metal milling technology due to the relatively high cost. And its photographs are illustrated in Fig. 24. In the fabrication process, the minimum radius of the drill is 0.1 mm. For the accuracy of assembly, the pins and screw holes of the UG-387/U flange are fabricated with high precision. Moreover, the fabricated structures are plated with 2 um thickness gold. The measurement of the filter-II is carried out with the Agilent Technologies PNA-X Network Analyzer N5245A, two OML WR-06 frequency extension modules, and a TRL calibration by the V06-AL-371 CalKit.

The simulated and measured results of the proposed filter-II are compared in Fig. 25. The measured FBW_{1dB} is 16.37% (128.58-151.5 GHz). The in-band reflection coefficient is better than -12.5 dB, the minimum insertion loss is around 0.33 dB, and the measured rectangle coefficient (BW_{40dB}/BW_{3dB}) is about 1.38. Experimental results agree well with the simulated results in general. It verifies that the frequency selectivity can be improved by cascading multiple over-mode cavities, and the insertion loss can be reduced by utilizing higher-mode cavities.

Table VI lists comparisons between the proposed filters and other high frequency filters. A good performance, including a wide bandwidth, a low insertion loss, and high selectivity, has been achieved by the proposed filters. The bandwidth and positions of TZs can be flexibly designed by properly selecting size of the proposed over-mode cavities and its operating modes. In addition, the implement of these higher-mode cavities helps to reduce the insertion loss and fabrication difficulty of the proposed filter, especially for THz applications. In general, the proposed filter-II has a simple structure, and exhibits a low insertion loss and high selectivity.

V. CONCLUSION

A low-loss mixed-mode filter with high selectivity based on the over-mode cavities has been proposed in this paper, and a simple design procedure is presented as well. The design of the proposed filter can be divided as several over-mode filtering block designs. Some empirical formulas have been given for quickly obtaining the initial geometries of each filtering block. The FBW and TZs' distributions can be flexibly designed by properly selecting size of the over-mode cavities and its operating modes. The frequency selectivity and out-of-band performance can be significantly improved by cascading several over-mode-cavity filtering blocks, which have different spurious passbands and TZs. The proposed filter has great potential in THz applications for its simple design procedure and high performance such as the low insertion loss and high frequency selectivity.

ACKNOWLEDGEMENT

Authors appreciate the SynMatrix Support Team [40] for their technical support in this work. Authors are very grateful of the help from Prof. Luca Perregrini from University of Pavia, Italy and Prof.

Cristiano Tomassoni from University of Perugia, Italy. They gave many valuable suggestions to explain clearly the operating principle of the proposed filter, which are very important to improve the quality of this work. In addition, authors also appreciate anonymous reviewers for their helpful comments.

REFERENCES

[1] S. Gu, C. Li, X. Gao, Z. Sun, and G. Fang, "Terahertz aperture synthesized imaging with fan-beam scanning for personnel screening," *IEEE Trans. Microw. Theory Techn.,* vol. 60, no. 2, pp. 3877-3885, Dec. 2012.

[2] S. Li *et al*., "Study of terahertz superresolution imaging scheme with real-time capability based on frequency scanning antenna," *IEEE Trans. THz Sci. Technol*., vol. 6, no. 3, pp. 451–463, May 2016.

[3] M. Lvovska, N. Seeman, R. Sha, T. Globus, T. Khromova, and T. Dorofeeva, "THz characterization of DNA four-way junction and its components," *IEEE Trans. Nanotechnology,* vol. 9, no. 5, pp. 610-617, Sep. 2010.

[4] D. Woolard, E. Brown, M. Pepper, and M. Kemp, "Terahertz frequency sensing and imaging: A time of reckoning future applications," *Proc. IEEE*, vol. 93, no. 10, pp. 1722-1743, Oct, 2005.

[5] K. Nallappan, H. Guerboukha, C. Nerguizian, and M. Skorobogatiy, "Live streaming of uncompressed HD and 4K videos using terahertz wireless links," *IEEE Access*, vol. 6, 2018.

[6] S. Mumtaz, J. M. Jornet, J. Aulin, W. H. Gerstacker, X. Dong, and B. Ai, "Terahertz communication for vehicular networks," *IEEE Trans. Veh. Technol*., vol. 66, no. 7, pp. 5617–5625, Jul. 2017.

[7] Z. W. Miao, Z. C. Hao, G. Q. Luo, J. Wang, X. Wang, and W. Hong, "140 GHz high-gain LTCC-integrated transmit-array antenna using a wideband SIW aperture-coupling phase delay structure," *IEEE Trans. Antennas Propag.*, vol. 66, no. 1, pp. 182-190, Jan. 2018.

[8] Z. W. Miao, Z. C. Hao, Y. Wang, B. B. Jin, J. B. Wu and W. Hong, "A 400-GHz high-gain quartz-based single-layered folded reflectarray antenna for terahertz applications," *IEEE Trans. THz Sci. Technol.,* vol. 9, no.1, pp.78-88, Jan. 2019.

[9] J. Zmuidzinas and P. L. Richards, "Superconducting detectors and mixers for millimeter and submillimeter astrophysics," *Proc. IEEE*, vol. 92, no. 10, pp. 1597–1616, Oct. 2004.

[10] K. K. Fan, Z. C. Hao, Q. Yuan, and W. Hong, "Development of a high gain 325–500 GHz antenna using quasi-planar reflectors," *IEEE Trans. Antennas Propag*., vol. 65, no. 7, pp. 3384–3391, May 2017.

[11] N. Zhang, R. Song, M. Hu, G. Shan, C. Wang, and J. Yang, "A low-loss design of bandpass filter at the terahertz band," *IEEE Microw. Wireless Compon. Lett*., vol. 28, no. 7, pp. 573–575, Jul. 2018.

[12] O. Glubokov, X. Zhao, J. Campion, U. Shah, and J. Oberhammer, "Micromachined filters at 450 GHz with 1% fractional bandwidth and unloaded Q beyond 700," *IEEE Trans. THz Sci. Technol*., vol. 9, no. 1, pp. 106–108, Jan. 2019.

[13] W. Liu *et al*., "Ultrabroad and angle tunable THz filter based on multiplexed metallic bar resonators," *IEEE Photonics Technology Letters*, vol. 30, no. 24, pp. 2103-2106, Dec. 2018.

[14] D. Koller, E. Bryerton, and J. Hesler, "WM380 (675-700 GHz) bandpass filter in milled, split-block construction," *IEEE Trans. THz Sci. Technol.*, vol. 8, no. 6, pp. 630–637, Nov. 2018.

[15] M. Stecher *et al*., "Polymeric THz 2D photonic crystal filters fabricated by fiber drawing," *IEEE Trans. THz Sci. Technol.*, vol. 2, no. 2, pp. 203–207, Mar. 2012.

[16] J. Li, H. Liu, and L. Zhang, "Compact and tunable-multichannel terahertz wave filter," *IEEE Trans. THz Sci. Technol*., vol. 5, no. 4, pp. 551–555, Jul. 2015.

[17] Z. Zhu *et al*., "A metamaterial-based terahertz low-pass filter with low insertion loss and sharp rejection," *IEEE Trans. THz Sci. Technol*., vol. 3, no. 6, pp. 832–837, Nov. 2013.

[18] V. Sanphuang, N. Ghalichechian, N. Nahar, and J. Volakis, "Reconfigurable THz filters using phase-change material and integrated heater," *IEEE Trans. THz Sci. Technol*., vol. 6, no. 4, pp. 583–591, Jul. 2016.

[19] R. Dickie, R. Cahill, V. Fusco, H. Gamble, and N. Mitchell, "THz frequency selective surface filters for earth observation remote sensing instruments," *IEEE Trans. THz Sci. Technol*., vol. 1, no. 2, pp. 450–461, Nov. 2011.

[20] J. Li, Y. Li, and L. Zhang, "Terahertz bandpass filter based on frequency selective surface," *IEEE Photonics Technology Letters*, vol. 30, no. 3, pp. 238-241, Feb. 2018.

[21] A. Khalil *et al*., "Quasi-elliptic and chebyshev compact LTCC multi-pole filters functioning in the submillimetric wave region at 150 GHz," *IEEE Trans. Microw. Theory Techn.,* vol. 58, no. 12, pp. 3925-3935, Dec. 2010.

[22] K. Wang, S. Wong, G. Sun, Z. Chen, L. Zhu, and Q. Chu, "Synthesis method for substrate-integrated waveguide bandpass filter with even-order chebyshev response," *IEEE Trans. Microw. Theory Techn.,* vol. 6, no. 1, pp. 126-135, Jan. 2016.

[23] S. W. Wong, K. Wang, Z. N. Chen, and Q. X. Chu, "Electric coupling structure of substrate integrated waveguide (SIW) for the application of 140-GHz bandpass filter on LTCC," *IEEE Trans. Compon., Packag., Manuf. Technol*., vol. 4, no. 2, pp. 316–322, Feb. 2015.

[24] Y. Li, L. A. Yang, L. Du, K. Zhang, and Y. Hao, "Design of millimeter-wave resonant cavity and filter using 3-D substrate-integrated circular waveguide," *IEEE Microw. Wireless Compon. Lett*., vol. 27, no. 8, pp. 706–708, Aug. 2017.

[25] X. H. Zhao et al., "D-band micromachined silicon rectangular waveguide filter," *IEEE Microw. Wireless Compon. Lett*., vol. 22, no. 5, pp. 230–232, May 2012.

[26] J. X. Zhuang, Z. C. Hao, and W. Hong, "Silicon micromachined terahertz bandpass filter with elliptic cavities," *IEEE Trans. THz Sci. Technol*., vol. 5, no. 6, pp. 1040–1047, Nov. 2015.

[27] K. M. K. H. Leong *et al*., "WR1.5 silicon micromachined waveguide components and active circuit integration methodology," *IEEE Trans. Microw. Theory Techn*., vol. 60, no. 4, pp. 998–1005, Apr. 2012.

[28] X. Shang, M. Ke, Y. Wang, and M. J. Lancaster, "Micromachined W-band waveguide and filter with two embedded H-plane bends," *IET Microwav., Antennas Propag*., vol. 5, no. 3, pp. 334–339, Feb. 2011.

[29] C. A. Leal-Sevillano, J. R. Montejo-Garai, M. Ke, M. J. Lancaster, J. A. Ruiz-Cruz, and J. M. Rebollar, "A pseudo-elliptical response filter at W-band fabricated with thick SU-8 photo-resist technology," *IEEE Microw. Wireless Compon. Lett*., vol. 22, no. 3, pp. 105–107, Mar. 2012.

[30] X. Shang, M. Ke, Y. Wang, and M. J. Lancaster, "WR-3 band waveguides and filters fabricated using SU8 photoresist micromachining technology," *IEEE Trans. THz Sci. Technol*., vol. 2, no. 6, pp. 629–637, Nov. 2012.

[31] H. Yang *et al*., "WR-3 waveguide bandpass filters fabricated using high precision CNC machining and SU-8 photoresist technology," *IEEE Trans. THz Sci. Technol*., vol. 8, no. 1, pp. 100–107, Jan. 2018.

[32] S. Mandal, H. O. Roy, L. B. Dubey, and A. K. Shukla, "Design and development of band pass filter at 140 GHz," *Intern. Conf. on Recent Adv. Microw. Theo. and App*., Jaipur, 2008, pp. 255-257.

[33] C. A. Leal-Sevillano, J. R. Montejo-Garai, J. A. Ruiz-Cruz, and J. M. Rebollar, "Low-loss elliptical response filter at 100 GHz," *IEEE Microw. Wireless Compon. Lett*., vol. 22, no. 9, pp. 459–461, Sep. 2012.

[34] J.-Q. Ding, S.-C. Shi, K. Zhou, Y. Zhao, D. Liu and W. Wu, "WR-3 band quasi-elliptical waveguide filters using higher order mode resonances," *IEEE Trans. THz Sci. Technol*., vol. 7, no. 3, pp. 302–309, May 2017.

[35] J. Q. Ding, S. C. Shi, K. Zhou, D. Liu, and W. Wu, "Analysis of 220-GHz low-loss quasi-elliptic waveguide bandpass filter," *IEEE Microw. Wireless Compon. Lett*., vol. 27, no. 7, pp. 648–650, Jul. 2017.

[36] Y. Xiao, P. Shan, K. Zhu, H. Sun, and F. Yang, "Analysis of a novel singlet and its application in THz bandpass filter design," *IEEE Trans. THz Sci. Technol*., vol. 8, no. 3, pp. 312–320, May 2018.

[37] C. Tomassoni, S. Bastioli, and R.V. Snyder, "Propagating waveguide filters using dielectric resonators," *IEEE Trans. Microw. Theory Techn*., vol. 63, no. 12, pp. 4366-4375, Dec. 2015.

[38] C. Tomassoni, S. Bastioli, and R.V. Snyder, "Compact mixed-mode filter based on TE_{101} cavity mode and $TE_{01\delta}$ dielectric mode," *IEEE Trans. Microw. Theory Techn*., vol. 64, no. 12, pp. 4434-4443, Dec. 2016.

[39] D.A. Taggart and R.D. Wanselow, "Mixed mode filters", *IEEE Trans. Microw. Theory Techn*., Vol. 22, pp. 898-902, Oct. 1974.

[40] *SynMatrix*. Accessed: Nov. 16, 2019. [Online]. Available: https://www.synmatrixtech.com/.